Journal of Non-Crystalline Solids 573 (2021) 121138

Contents lists available at ScienceDirect

Journal of Non-Crystalline Solids

journal homepage: www.elsevier.com/locate/jnoncrysol

Revealing the medium-range structure of glassy silica using force-enhanced atomic refinement

Qi Zhou [a,b], Ying Shi [a], Binghui Deng [a], Tao Du [c], Lijie Guo [d,*], Morten M. Smedskjaer [c], Mathieu Bauchy [b,*]

[a] Science and Technology Division, Corning Incorporated, Corning, NY 14831, USA
[b] Physics of AmoRphous and Inorganic Solids Laboratory (PARISlab), Department of Civil and Environmental Engineering, University of California, Los Angeles CA 90095, USA
[c] Department of Chemistry and Bioscience, Aalborg University, Aalborg 9220, Denmark
[d] National Center for International Research on Green Metal Mining, BGRIMM Technology Group, Beijing 100160, China

ARTICLE INFO

Keywords:
Glassy silica
Atomic structure
Molecular dynamics
Reverse Monte Carlo modeling
Medium-range order

ABSTRACT

The medium-range order structure of silicate glasses remains poorly known as it is not directly visible from conventional experiments. In turn, although atomistic simulations offer a direct access to the structure of glasses, they face several limitations, e.g., extremely high cooling rates. Here, we adopt the force-enhanced atomic refinement (FEAR) method to overcome these limitations and reveal the atomic structure of glassy silica, both at the short- and medium-range length scales. We find that FEAR yields a glass structure that simultaneously exhibits higher thermodynamic stability and enhanced agreement with experimental structure data as compared with molecular dynamics and reverse Monte Carlo simulations. Overall, we show that the increased stability enabled by FEAR primarily arises from the fact that the generated atomic configuration exhibits a more ordered medium-range structure and a lower fraction of unstable small silicate rings.

1. Introduction

Despite the ubiquity and technological importance of silicate glasses [1–4], their atomic structure remains only partially understood [5]. In that regard, even the structure of pure glassy silica (SiO_2) remains subject to debate [6]. The short-range order base structure of SiO_2 is well understood, with SiO_4 tetrahedral units that are interconnected via bridging-oxygen atoms [7]. At larger distances, the SiO_4 polytopes form some closed-loop rings, which largely dictates silica's medium-range order [8,9]. However, even basic features of silica's medium-range order (e.g., ring size distribution) remain debated [10,11].

This lack of knowledge regarding the atomic structure of glassy silica—especially at the medium-range order—partially arises from the lack of experimental techniques that can directly probe the atomic structure of silicate glasses [12], although recent developments offer exciting perspectives in that regard [13]. Indeed, even though conventional experiments can offer useful "fingerprints" of the glass structure, they often do not provide a direct access to the atomic structure itself [14]. For instance, diffraction experiments offer some signatures of the medium-range order of silicate glasses, e.g., as captured by the first-sharp diffraction peak (FSDP) [15–17]. Although this information places some constraints on the nature of the medium-range order, it does not directly reveal the medium-range order structure itself—e.g., it does not provide a direct access to the ring size distribution [18].

As an alternative route to experiments, atomistic simulations offer a direct and full access to the atomic structure of glasses [19–21] and, hence, can reveal some atomic details that are invisible to conventional experiments [6,19,22]. However, atomistic simulations come with their own challenges and limitations [23,24]. On the one hand, molecular dynamics (MD) simulations solely rely on the knowledge of the interatomic forcefield. Following the melt-quench method, melts are equilibrated at high temperature to lose the memory of their initial configuration and subsequently quenched to the glassy state with a high cooling rate [21,25,26]. Although this melt-quenching approach roughly mimics the experimental synthesis protocol of glasses, MD simulations are limited to very large cooling rates (typically 10^2 to 10^{-2} K/ps) due to their computational cost [27]. This is a serious limitation since, as out-of-equilibrium materials, the structure and properties of glasses depend on their thermal history [25]. In that regard, glasses simulated by MD using the conventional melt-quench approach

* Corresponding authors.
E-mail addresses: guolijie@bgrimm.com (L. Guo), bauchy@ucla.edu (M. Bauchy).

https://doi.org/10.1016/j.jnoncrysol.2021.121138
Received 24 June 2021; Received in revised form 10 August 2021; Accepted 19 August 2021
Available online 26 August 2021

typically exhibit a larger fictive temperature than their experimental counterparts, which, in turn, causes their structure to be unrealistically disordered (especially at the medium-range order) [21,23,26,28–32]. On the other hand, conventional reverse Monte Carlo (RMC) simulations solely rely on the knowledge of some experimental constraints (e.g., experimental pair distribution function) [33–35]. As a key advantage, RMC simulations can yield glasses structures that are compatible with such constraints while bypassing the melt-quenching route, thereby avoiding the issue of the cooling rate [36–39]. However, a RMC simulation remains an ill-defined problem, since, for instance, numerous atomic structures can exhibit the same pair distribution function [40]. As such, glass structures that are generated by RMC typically exhibit an excellent agreement with the experimental data that are used as constraints during the refinement, but may nevertheless be fairly unrealistic (e.g., showing extremely high potential energy) [41]. Overall, these challenges limit the ability of atomistic simulations to provide fully trustable atomic structures for silicate glasses.

To address this challenge, Drabold et al. recently introduced a new atomic refinement approach that seamlessly combine the knowledge of (i) the interatomic forcefield (which is typically used by MD simulations) and (ii) experimental constraints (which are typically used by RMC simulations) [42]. In detail, Drabold's force-enhanced atomic refinement (FEAR) method relies on an iterative combination of sequential RMC refinements and energy minimizations [14,41–43]. Unlike hybrid RMC approaches—which simultaneously refine the experimental constraints and minimize the energy through a single, unified cost optimization function accounting for both experimental constraints and energy—FEAR does not rely on any arbitrary choices regarding the weights attributed to energy and experimental constraints. The fact that the energy of the system is only computed during the energy minimizations steps (rather than at every step in hybrid RMC approaches) also results in enhanced overall computational efficiency [42].

Recently, we demonstrated that FEAR yields an atomic structure for a sodium silicate glass that is more realistic than that offered by MD or RMC [41]. In this contribution, we extend this approach to the archetypical case of glassy silica. Indeed, despite its apparent simplicity as compared to modified silicate glasses like sodium silicate, glassy silica comes with unique challenges. In particular, the structure and properties of silica have been shown to be more affected by the cooling rate than those of sodium silicate [44]. Here, we show that the SiO_2 structure generated by FEAR simultaneously (i) exhibits an excellent agreement with experimental data and (ii) is more energetically stable than those obtained by MD or RMC simulations. This allows us to investigate the nature of the medium-range order structure in glassy silica.

2. Methods

2.1. Simulated system

In the following, we compare the ability of MD, RMC, and FEAR to offer a realistic description of the atomic structure of glassy silica, which is an archetypical model glass and offers a structural basis for more complex modified silicate glasses. The simulated system comprises 3000 atoms. For this system, we adopt the Beest–Kramer–Santen (BKS) forcefield [45], which has been extensively used to investigate the structure, dynamics, and thermodynamics of silica [21,26,44]. In line with previous studies, we use a cutoff of 5.5 Å and 10.0 Å for the short-range and long-range Coulombic interactions, respectively [26,46]. The long-range Coulombic interactions are evaluated with the Particle- Particle Mesh (PPPM) algorithm [47] with an accuracy of 10^{-5}—wherein the PPPM approach relies on the particle mesh method, which consists of interpolating the particles onto a three-dimensional grid for improved computational efficiency.

In order to further assess whether or not the outcome of the FEAR method depends on the choice of the interatomic potential (i.e., BKS) used during the energy minimizations, we repeat the FEAR simulations while using selected alternative forcefields, namely, the interatomic potentials from Guillot and Sator [48] and Pedone et al. [49]. We select these potentials as, although they all present a two-body formulation, they rely on different analytical forms, different parameterizations, and different partial charges (i.e., the charges attributed to Si and O atoms). Note that, to ensure consistency, all the other simulation parameters are kept identical. All simulations are carried out using the Large-scale Atomic/Molecular Massively Parallel Simulator (LAMMPS) package [50].

2.2. Melt-quenching simulations by molecular dynamics (MD)

To establish benchmark silica structures that can be compared with that generated by FEAR, we first prepare a series of glassy silica structures by melt-quenching using MD simulations, as detailed in the following. An initial silica configuration is first created by randomly placing the atoms in a cubic box while ensuring the absence of any unrealistic overlap. The system is then melted at 5000 K under zero pressure in the isothermal-isobaric (*NPT*) ensemble for 100 ps to ensure the complete loss of the memory of the initial configuration. The melt is then linearly cooled down to 300 K under zero pressure in the *NPT* ensemble with varying cooling rates ranging from 10^2 down to 10^{-2} K/ps. For all simulations, we adopt the Nosé–Hoover thermostat and a fixed timestep of 1 fs [51].

2.3. Reverse Monte Carlo (RMC) simulations

As a second benchmark, we then use experimental neutron diffraction data [52] to create a glassy silica structure by RMC simulation [33,34], as implemented through an in-house fix in LAMMPS. This method iteratively refines the position of the atoms in a simulation box until the glass exhibits a structure that matches target experimental data—here, we use the neutron pair distribution function (PDF) sourced from Ref. [52] as experimental constraint. To compare the simulated structure with neutron diffraction data, we first calculate the neutron PDF $g_N(r)$ of the simulated structures by combining the partial PDFs $g_{ij}(r)$ as:

$$g_N(r) = \frac{1}{\sum_{i,j=1}^{n} c_i c_j b_i b_j} \sum_{i,j=1}^{n} c_i c_j b_i b_j g_{ij}(r) \quad (1)$$

where c_i are the molar fractions of element i (i = Si or O), b_i are the neutron scattering lengths of the species [53] (equal to 4.1491 and 5.803 fm for Si and O atoms, respectively), and r is the real-space distance. Note that, to ensure a meaningful comparison between simulated and experimental PDFs, the simulated PDFs need to be broadened [54]. Here, this is achieved by convoluting the computed PDFs with a normalized Gaussian distribution with a full width at half-maximum (FWHM) given by FWHM = $5.16/Q_{max}$ [25], where Q_{max} is the maximum wave vector used in the diffraction test (here, $Q_{max} = 50$ Å^{-1}). The level of agreement between the simulated and experimental PDFs is then captured by the R_χ factor proposed by Wright (which is here calculated over r = 0-to-10 Å) [54]:

$$R_\chi^2 = \sum_i \left[g^{exp}(r_i) - g^{sim}(r_i)\right]^2 \Big/ \left(\sum_i g^{exp}(r_i)\right)^2 \quad (2)$$

The RMC method is used to "invert" the experimental neutron pair distribution into a three-dimensional atomic structure. This method includes the following steps. (i) Starting from an initial random structure (identical to that used for the MD simulation), we first calculate the pair distribution function of the simulated structure and the Wright's coefficient R_χ^{old} (see Eq. 2). (ii) An atom is randomly selected and then displaced with a random direction and distance. (iii) The pair distribution function of the new configuration and the new coefficient R_χ^{new} are calculated. (iv) Following the Metropolis algorithm, the new configuration is accepted if $R_\chi^{new} \leq R_\chi^{old}$, that is, if the level of agreement

between simulated and experimental structure is improved by the Monte Carlo move. If not, the atomic displacement is accepted with a certain probability P shown below or refused otherwise:

$$P = \exp\left[-\frac{R_\chi^{\text{new}^2} - R_\chi^{\text{old}^2}}{T_\chi}\right] \tag{3}$$

where T_χ plays the role of a (unitless) "effective temperature" that controls the probability of acceptance (that is, higher values of T_χ result in higher probability of acceptance of the Monte Carlo moves). Here, the term $(R_\chi^{\text{new}^2} - R_\chi^{\text{old}^2})/T_\chi$ is equivalent to the quantity $(U^{\text{new}} - U^{\text{old}})/kT$ in the conventional energy-based Metropolis algorithm, where U is the energy of the system—wherein, here, the Wright's coefficient R_χ plays the role of an "effective energy." Here, we use $T_\chi = 0.01$, which is found herein to result in the lowest final R_χ value upon convergence. Atomic displacements and directions are randomly chosen, with a uniform displacement probability distribution between 0 and 0.2 Å. The simulation box size is kept fixed throughout the simulation, with a length of 35.248 Å, so that density is fixed according to the experimental value of 2.20 g/cm^3. A total number of 140,000 RMC moves are attempted until convergence.

2.4. Force-enhancement atomic refinement (FEAR) simulation

Finally, we assess the ability of the FEAR refinement method to offer an improved description of the atomic structure of glassy silica as compared to those generated by MD or RMC. To this end, we adopt the FEAR methodology introduced by Drabold et al. [42], which is here implemented via an in-house fix in LAMMPS. To ensure a meaningful comparison between FEAR, RMC, and MD, all simulated systems have the same size, and all simulation parameters are kept identical (e.g., forcefield, cutoff, etc.). In detail, we first start from a "randomized" structure generated by RMC while using a very high effective temperature, namely, $T_\chi = 5000$. Following the original implementation of the FEAR method, the system is then iteratively subjected to a combination of RMC refinements and energy minimization steps, wherein each FEAR iteration consists of (i) 3000 RMC steps and (ii) an energy minimization (conducted with the conjugated gradient method). We find that 20 of such iterations are sufficient to achieve a convergence of potential energy and R_χ for glassy silica. During the refinement, we dynamically adjust the average acceptance probability of the Metropolis algorithm by linearly decreasing the effective temperature T_χ from 10^3 down to 10^{-4} during the course of the FEAR refinement. These parameters are found to yield a glass structure exhibiting minimum R_χ and potential energy values. When comparing FEAR vs. RMC, it should be noted that there exist some RMC-based approaches that are more elaborated than the RMC simulation used herein. For instance, the hybrid reverse Monte Carlo approach (HRMC) consists in explicitly adding the computed potential energy of the system as an additional contribution in the RMC cost function to be minimized [36,37]. Although such advanced approaches can likely offer accuracies that are competitive with that offered by FEAR [41], FEAR presents two key advantages: (i) it is more computationally efficient since the energy does not need to computed at every RMC step and (ii) it does not rely on any assumption regarding the weights associated with the structural and energy terms in the cost function.

2.5. Short-range order structural analysis

We analyze the short-range order radial environment around each atom by computing the partial PDFs. In addition, we explore the short-range angular environment of the atoms by computing the partial bond angle distribution (PBAD) using the RINGS package [55]. Specifically, we focus on the O–Si–O and Si–O–Si PBADs, which characterize the intra- and inter-polytope angular structure of the SiO_4 tetrahedral units, respectively. The distance cutoff used to define the Si–O bonds is chosen as the position of the first minimum after the first peak of the partial Si–O PDF (1.90 Å).

2.6. Medium-range order structural analysis

To further explore the structure of glassy silica over intermediate length scales, we calculate the partial structure factors $S_{ij}(Q)$ from the Fourier transform of the partial PDFs:

$$S_{ij}(Q) = 1 + \rho_0 \int_0^R 4\pi r^2 \left(g_{ij}(r) - 1\right) \frac{\sin(Qr)}{Qr} dr \tag{4}$$

where Q is the scattering vector, ρ_0 is the average atomic number density, and R is the integration cutoff (half of the simulation box length). The total neutron structure factor is then evaluated by combining the partial structure factors as follows:

$$S_{\text{N}}(Q) = \left(\sum_{i,j=1}^{n} c_i c_j b_i b_j\right)^{-1} \sum_{i,j=1}^{n} c_i c_j b_i b_j S_{ij}(Q) \tag{5}$$

To further magnify high-Q fluctuations in the structure factor, we then calculate the reduced structure factor:

$$F(Q) = Q[S(Q) - 1] \tag{6}$$

Finally, to further explore the medium-range order structure of glassy silica, we compute the ring size distribution of each simulated system by using the RINGS package [55], wherein rings are defined as the shortest closed paths within the glassy silica network. The size of a ring is here defined in terms of the number of Si atoms it comprises. Here, we use the Guttman definition for the calculation [56]. This definition was chosen as it yields, on average, the expected value of 6 rings per Si atom [18,29]. We adopt a maximum ring size of 7, since no larger rings are found in the simulated structures (with the Guttman criterion).

3. Results

3.1. Evolution of structure upon force-enhanced atomic refinement

Fig. 1 shows selected snapshots of the atomic structure of the simulated silica glass upon FEAR refinement. Si–O bonds (i.e., when the distance between a Si/O pair of atoms is lower than the 1.9 Å cutoff) are shown as edges in the snapshots. We observe that, the degree of connectivity (i.e., the number of Si–O bonds) increases during refinement.

Fig. 2**a** shows the neutron PDF of the three structures shown in Fig. 1, that is, after different increasing numbers of FEAR refinement steps. The computed PDFs exhibit all the typical features that are expected for an SiO_2 glass, namely, (i) a first peak around 1.6 Å that corresponds to Si–O correlations, (ii) a second peak around 2.7 Å associated to O–O correlations, and (iii) a plateau toward 1 at long r-distance, which is indicative of the absence of any long-range order. Overall, all these PDFs show a fair agreement with available experimental neutron diffraction data [52] in terms of the positions of the first and second peaks. This indicates that, even at early stage of the FEAR refinement, the simulated structures exhibit a realistic description of the interatomic distances in SiO_4 tetrahedra. Nevertheless, we observe that, initially, the peaks of the computed PDF are notably broader than those of the experimental PDF. This indicates that, initially, the simulated structure is unrealistically disordered. Upon FEAR refinement, we observe that the shape of the first peak becomes reasonably well described (in terms of position, intensity, and width) after about 10 FEAR iterations, whereas the second peak becomes well reproduced after about 15 FEAR iterations. This suggests that the short-range order (i.e., low-distance correlations) is refined faster than the medium-range order (i.e., intermediate-distance

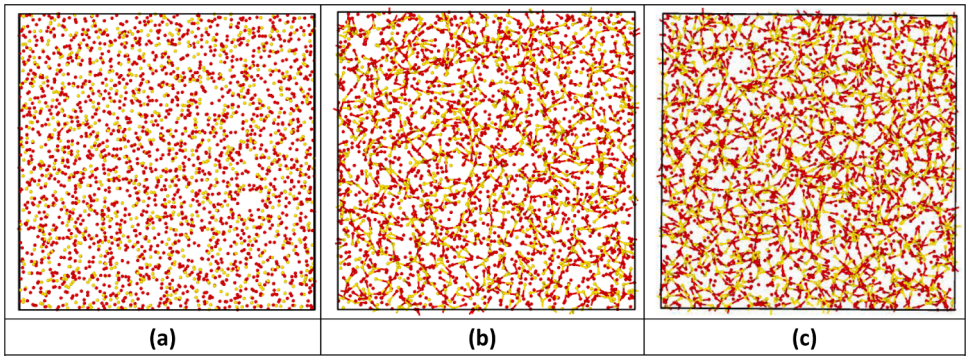

Fig. 1. Snapshots of the simulated glassy silica structures obtained after **(a)** 1, **(b)** 10, and **(b)** 20 iterations of force-enhanced atomic refinement (FEAR). Si–O bonds (i.e., when the distance between a Si/O pair of atoms is lower than the 1.9 Å cutoff) are shown as edges.

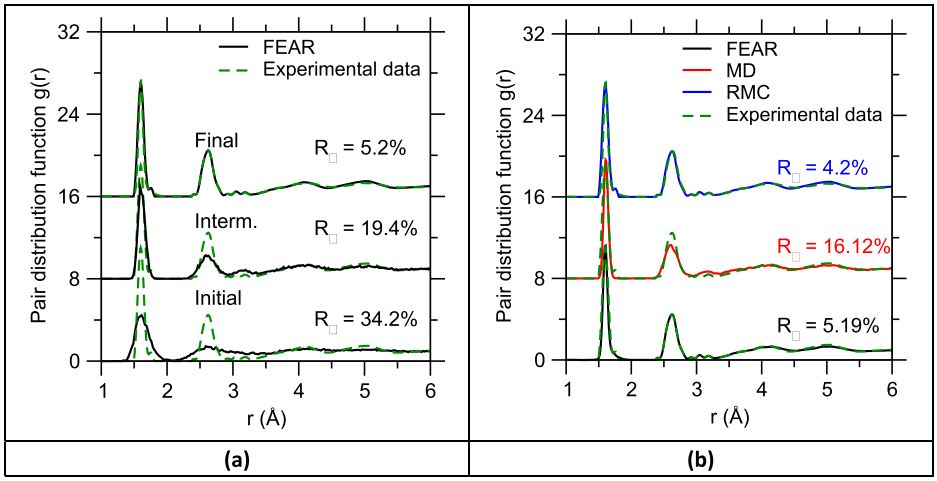

Fig. 2. **(a)** Neutron pair distribution functions (PDFs) of the glassy silica structures formed by force-enhanced atomic refinement (FEAR) that are shown in Fig. 1. **(b)** Neutron PDFs of the final glassy silica structures generated by FEAR, molecular dynamics (MD, using a standard cooling rate of 1 K/ps), and reverse Monte Carlo (RMC). All the PDFs are compared with the same experimental neutron diffraction data [52].

correlations). This can be understood from the fact that refining the short-range order only involves some slight displacements of the neighbors of each atom, which only requires small energy barriers to be overcome. In contrast, refining the medium-range order requires some collective atomic displacements, including the breakage and formation of interatomic bonds, which requires hopping over higher energy barriers.

After 20 FEAR iterations, we observe that the PDF of the final simulated configuration shows an excellent agreement with experimental neutron data, both for the short and medium-range length scales.

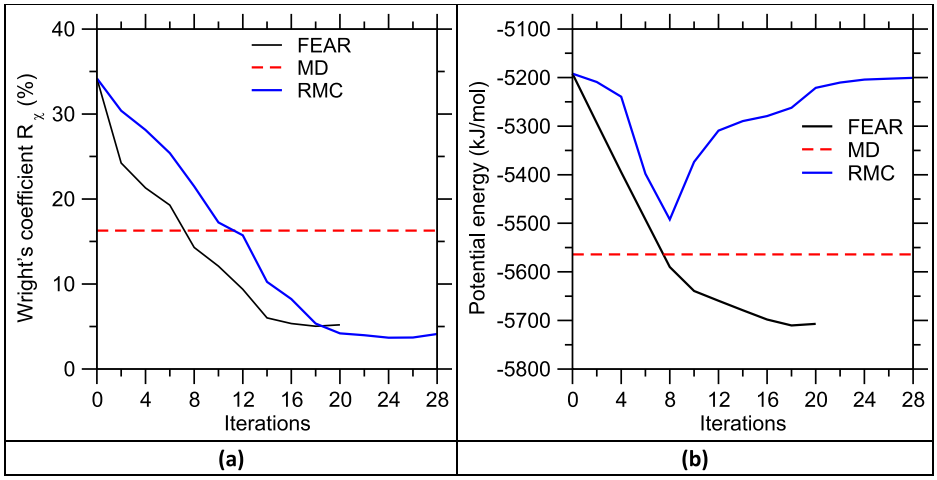

Fig. 3. **(a)** Wright's coefficient R_χ and **(b)** molar potential energy as a function of the number of iterations of force-enhanced atomic refinement (FEAR) and reverse Monte Carlo (RMC) refinement. Values obtained for a melt-quenched glass generated by molecular dynamics (MD) with a standard cooling rate of 1 K/ps are shown as horizontal dashed lines for comparison.

As a measure of the level of agreement between simulations and experiments, we find that, at the end of the refinement, the Wright factor R_χ reaches a value of 5.2%. We note that this value is higher than the one that we previously obtained upon FEAR refinement of a sodium silicate glass [41], which highlights the unique challenges associated with the structure of glassy silica. Nevertheless, this final value is judged as satisfactory since R_χ values that are lower than 10% are typically considered to be indicative of a good agreement between simulations and experiments [54]

3.2. Comparison with molecular dynamics and reverse Monte Carlo

First, we compare the glass structure generated by FEAR with that offered by RMC. Fig. 3**a** shows the evolution of the R_χ factor of the glass structure upon RMC refinement. We observe that the R_χ factor monotonically decreases and eventually reaches a final value of 4.2%, which is slightly lower than the value achieved by FEAR. This only indicates that RMC yields a pair distribution function that is in very good agreement with experimental neutron diffraction data (see Fig. 2**b**). Such high level of agreement is not surprising since RMC refinement solely aims to decrease R_χ (i.e., R_χ is the only cost function during refinement). It is worth noting that, since they comprise energy minimization steps, FEAR simulations come with an additional computational burden as compared to traditional RMC. However, since the energy minimization is herein only performed every 3000 RMC steps, the computational cost of FEAR simulations remains fairly dominated by the RMC steps. In practice, for a constant number of 20 (RMC or FEAR) iterations, a single simulation conducted on a single core of an Intel Xeon E5-2600 V2 processor is found to require 75h27 and 72h10 for FEAR and RMC, respectively—so that FEAR involves a 4.8% increase in computing cost. Nevertheless, we note that RMC requires slightly more iterations than FEAR to converge. This suggests that periodically minimizing the energy of the simulated structure (i.e., as done during FEAR refinement) effectively accelerates the refinement, that is, it decreases the number of RMC steps that are needed to achieve convergence—in line with previous findings [41]. Overall, these results highlight the computational efficiency of the FEAR approach.

Fig. 2**b** shows the neutron PDF of the glass structure generated by the melt-quench MD approach. We note that the PDF offered by MD only matches well with neutron diffraction data at low distance (i.e., for the first peak in the PDF), which indicates that MD offers a realistic description of the Si–O interatomic distance. Nevertheless, we find that, overall, MD yields a notably decreased level of agreement with experimental neutron diffraction data at larger distances (as compared to FEAR and RMC), which is illustrated by the larger value of the R_χ factor (16.1%, see Fig. 3**b**). The discrepancy between the experimental and MD-based PDFs mostly manifests itself in the second peak of the PDF, indicating that, in contrast with FEAR and RMC, MD partially misrepresents second-neighbor (O–O and Si–Si) correlations within the glass structure.

Next, we focus on the thermodynamic stability of the configuration generated by FEAR, RMC, and MD. Fig. 3**b** shows the evolution of the molar potential energy of the system upon RMC refinement. Overall, we observe that RMC yields a potential energy that is significantly higher than that offered by the other simulation approaches. Specifically, the molar potential energy of the structure generated by RMC is eventually about 360 kJ/mol larger than that of the structure simulated by MD. This is not surprising since RMC does not consider the interatomic energy of the system in its cost function. However, such high energy exemplifies the fact that, although the PDF calculated from the glass structure generated by RMC offers an excellent match with experimental neutron diffraction data, the configuration yielded by RMC is thermodynamically unstable. This echoes the fact the PDF is not a very discriminative metric to evaluate the soundness of a glass structure, that is, various structures featuring very different energies can nevertheless feature similar PDFs. Overall, these results indicate that, despite the apparent agreement with neutron diffraction data, RMC does not yield a realistic structure for glassy silica.

In contrast, Fig. 3**b** shows that FEAR eventually yields a potential energy that is significantly lower than that offered by both RMC and MD simulations. This is a key result since it implies that, although FEAR and MD rely on the same interatomic forcefield, the FEAR refinement scheme allows the simulated glass to reach more stable energy states. This arises from the fact that, during MD-based melt-quenching, the simulated glass quickly gets trapped within a given basin of the energy landscape as temperature decreases [57]. The low value of the thermal activation then prevents the glass from escaping for this basin—so that the simulated glass retains a large fictive temperature (i.e., high-energy state). In contrast, upon FEAR refinement, the RMC steps that are performed in between each energy minimization tend to induce some slight structural perturbations that allow the simulated glass to overcome some large energy barriers that would be inaccessible during the limited timescale of MD simulations and, thereby, to reach deeper basins within the energy landscape. This establishes FEAR as a powerful method to generate simulated glass structures that are more stable than those created by MD. Overall, these results show that FEAR refinement can produce glass structures that simultaneously feature an unprecedented level of agreement with experimental neutron diffraction data and increased energetic stability.

It is insightful to compare the differences in R_χ and potential energy yielded by the different simulation techniques considered herein with the level of variation that results from the use of different cooling rates in melt-quench MD simulations. To this end, Fig. 4**a** first shows the metric R_χ offered by MD simulations as a function of the cooling rate. As expected, R_χ decreases upon decreasing cooling rate. This indicates that, as the cooling rate decreases, the glass structure produced by MD gradually converges toward the experimental neutron diffraction data. On the other hand, independently of the cooling rate, the R_χ coefficient of the glass structures simulated by MD remains significantly higher than those obtained by RMC and FEAR refinement. In agreement with previous results [41], we find that the evolution of R_χ as a function of the cooling rate can be well described by a power law function—in line with mode-coupling theory [58]. Using as a reference the power law relationship fitted based on the R_χ vs. cooling rate data obtained from MD (see Fig. 4**a**), we find, by extrapolation, that a cooling rate of about 10 K/s (i.e., 10^{-11} K/ps, vs. 10^{-2} K/ps for the longest MD simulation considered herein) would be needed for the MD simulation to yield an R_χ coefficient that is comparable to that offered by FEAR. Although this cooling rate echoes typical experimental values, it is completely out-of-reach from MD simulations. These results highlight that the FEAR approach is able to generate atomic configurations that are comparable to well-annealed glass structures formed using slow cooling rates.

Fig. 4**b** presents the evolution of the molar potential energy of the MD-simulated glasses as a function of the cooling rate. We observe that the potential energy decreases upon decreasing cooling rate. As expected, this implies that, as the cooling rate decreases, the system becomes more stable and be able to reach a deeper state within the energy landscape [57]. Notably, even at the highest cooling rate (100 K/ps), the energy of the glass simulated by MD remains significantly lower than that of the RMC-based glass. This further illustrates the unrealistic nature of the glass generated by RMC. In contrast, we find that the energy of the glass generated by FEAR remains systematically lower than those of the glasses simulated by MD, even in the case of the slowest cooling rate (0.01 K/ps). This further confirms that FEAR yields a very stable glass structure that is associated with a low fictive temperature.

3.3. Effect of force-enhanced refinement on the short-range structure

In the following, we explore how the increased thermodynamic stability of the glass generated by FEAR is encoded in its structure. We

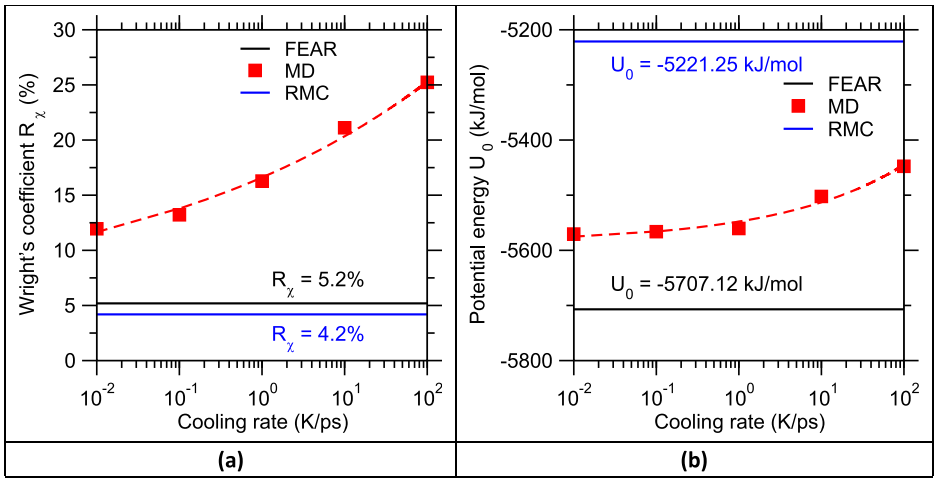

Fig. 4. **(a)** Wright's coefficient R_χ and **(b)** molar potential energy of melt-quenched glasses generated by molecular dynamics (MD) simulations as a function of the cooling rate. The dashed lines are some power law fits to guide the eye. Values obtained for the glasses generated by force-enhanced atomic refinement (FEAR) and reverse Monte Carlo (RMC) are shown as horizontal lines for comparison.

first focus on the short-range order (<3.5 Å) structure. Fig. 5 shows the Si–O, O–O, and Si–Si partial PDFs obtained by MD, RMC, and FEAR. We first observe that the first peak in the Si–O and O–O partial PDFs (around 1.6 and 2.6 Å, respectively) remains largely similar in the three simulated glasses. This indicates that FEAR refinement does not notably affect the average Si–O and O–O interatomic distances, which are already well predicted by MD and RMC (see **Table 1**). These average interatomic distances are in good agreement with available experimental data [59]. In contrast, we find that, when compared with the MD-based glass, the Si–Si peak shifts toward higher distance upon FEAR refinement. This signals that, as compared to MD, FEAR predicts a higher average Si–Si interatomic distance, which exhibits an excellent match with experimental data (see **Table 1**) [59]. Since the Si–O average distance remains constant, the increase in the Si–Si distance arises from an increase in the Si–O–Si angle (see below). In addition, the first Si–Si peak offered by FEAR is sharper than those predicted by MD and RMC. This indicates that FEAR yields a more pronounced degree of ordering between neighboring SiO_4 tetrahedra than MD and RMC, which may explain the increased stability of the glass generated by FEAR.

Then, we direct our attention to the short-range angular environment of each element. Fig. 6 shows the O–Si–O (i.e., intratetrahedral) and Si–O–Si (i.e., intertetrahedral) PBADs offered by FEAR, RMC, and MD. We first note that the average O–Si–O angles predicted by these three simulation methods remain largely similar (around 109°). This value matches with available experimental data (see **Table 2**). This signals that the tetrahedral environment of Si atoms is already well-defined by MD and that FEAR does not induce any notable further refinements. However, we note that the O–Si–O PBAD becomes sharper upon FEAR refinement. This indicates that FEAR predicts a more ordered angular environment for Si atoms, while in turn, MD and RMC yield more distorted SiO4 tetrahedral. This echoes the fact that, based on previous MD results, the O–Si–O PBAD tends to become sharper upon decreasing cooling rate, that is, as the glass becomes more stable [25].

We then focus on the Si–O–Si PBAD. We find that the Si–O–Si PBAD

Table 1
Average Si–O, O–O, and Si–Si interatomic distance values computed by force-enhanced atomic refinement (FEAR), molecular dynamics (MD), and reverse Monte Carlo (RMC) simulation. Experimental values sourced from Ref. [59] are provided for comparison.

	Si–O (Å)	O–O (Å)	Si–Si (Å)
FEAR	1.611	2.624	3.067
MD	1.598	2.590	2.962
RMC	1.582	2.593	3.127
Experimental data	1.608 ± 0.004	2.626 ± 0.006	3.077

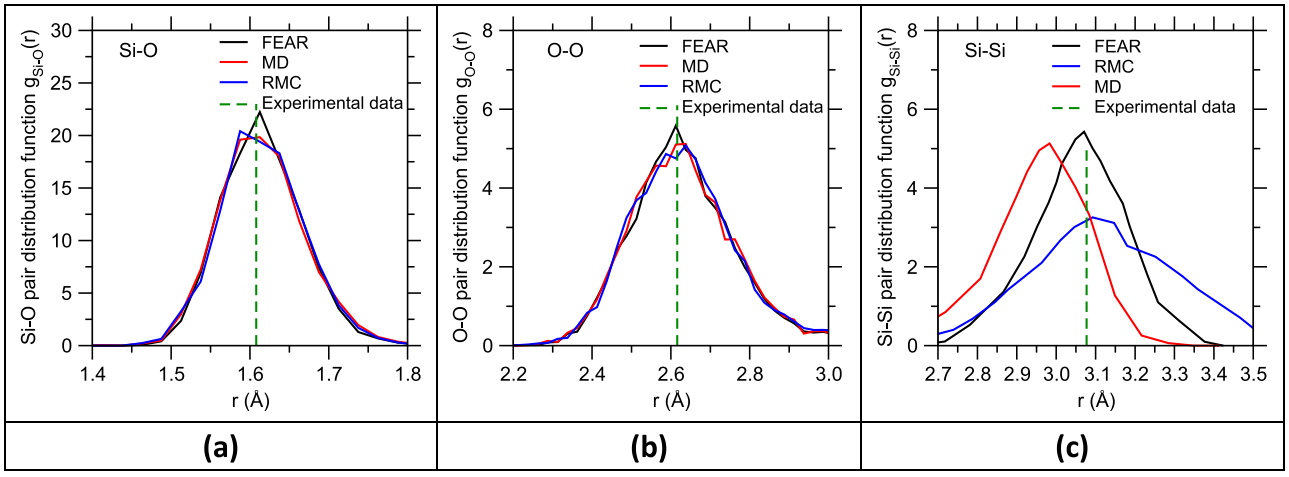

Fig. 5. **(a)** Si–O, **(b)** O–O, and **(c)** Si–Si partial pair distribution functions computed by force-enhanced atomic refinement (FEAR), molecular dynamics (MD, using a cooling rate of 1 K/ps), and reverse Monte Carlo (RMC) simulation. The vertical dashed lines indicate experimental interatomic distances sourced from Ref. [59].

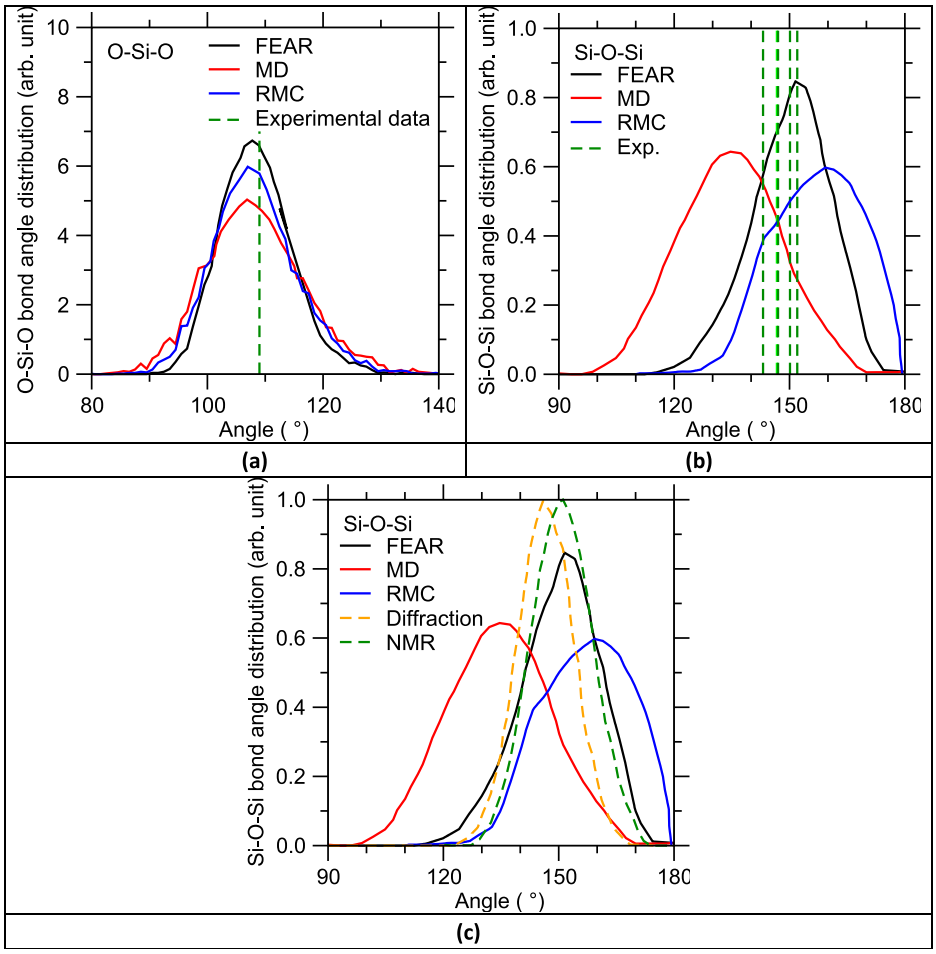

Fig. 6. (a) O–Si–O and **(b)** Si–O–Si partial bond angle distributions computed by force-enhanced atomic refinement (FEAR), molecular dynamics (MD, using a standard cooling rate of 1 K/ps), and reverse Monte Carlo (RMC) simulation. The vertical dashed lines indicate experimental average angle values obtained from different experimental data [61–65] **(c)** Si–O–Si partial bond angle distributions computed by FEAR, MD, and RMC simulation, which are compared with reference PBADs computed from combined neutron and photon diffraction [60] and nuclear magnetic resonance (NMR) experimental data [62].

Table 2
Average interatomic angle values computed by force-enhanced atomic refinement (FEAR), molecular dynamics (MD, using a cooling rate of 1 K/ps), and reverse Monte Carlo (RMC) simulation. Computed data are compared with experimental values sourced from Refs. [60–64], which are based on X-ray diffraction (XRD), high-energy X-ray diffraction (HXRD), and ^{29}Si Nuclear magnetic resonance (NMR) spectroscopy data. The full-width at half-maximum (FWHM) of the Si–O–Si partial bond-angle distribution is also indicated for comparison.

	O–Si–O	Si–O–Si	FWHM of Si–O–Si
FEAR	109.2°	152.9°	23.4°
MD	107.6°	137.4°	31.8°
RMC	108.6°	161.6°	34.2°
Combined neutron and photon diffraction [60]	109.47°	148.3°	17.2°
^{29}Si NMR [61]	109.47°	150.1°	21.4°
^{29}Si NMR [62]	109.7°	151°	18.7°
HXRD [63]	109.3°	147°	35.5°
Combined neutron and x-ray [64]	109.47°	141°	22.1°

offered by FEAR exhibits a notable shift as compared to MD and RMC data. The average Si–O–Si angle predicted by FEAR is significantly larger than that predicted by MD. The opening of the Si–O–Si angle predicted by FEAR is in agreement with the larger Si–Si distance observed in Fig. 5**c** and is well supported by available experimental data [52,60–64] The shift of the Si–O–Si angle toward larger values also echoes the fact that, based on previous MD results, this angle tends to increase upon decreasing cooling rate, that is, as the glass reaches lower fictive temperatures [25]. We also note that FEAR yields a sharper Si–O–Si PBAD than MD, which, once again, matches with the fact that, based on previous MD results, this PBAD tends to sharpen upon decreasing cooling rate [25]. This is also in agreement with the sharp PBAD that was inferred from experimental nuclear magnetic resonance (NMR) data in Ref. [64] (see Fig. 6**c**). This sharpening of the Si–O–Si PBAD indicates that FEAR predicts an increased degree of ordering in between neighboring SiO_4 tetrahedra compared to MD and RMC. Overall, the distinctive features of the short-range order of the glass yielded by FEAR are all supported by experimental data and offer a structural basis for the increased thermodynamic stability of the glass generated by FEAR.

3.4. *Effect of force-enhanced refinement on the medium-range structure*

Finally, we explore how the increased thermodynamic stability of the glass generated by FEAR manifests itself in its medium-range order structure of the simulated glass structure. To this end, we compute the neutron structure factor for each of the simulated glasses (see Section 2.6). Fig. 7 shows the reduced structure factor predicted by FEAR, RMC, and MD, which are compared with neutron diffraction data [52]. We first observe that all the simulation techniques considered herein (MD, RMC, and FEAR) offer a realistic prediction of the glass structure factor, since the positions of the peaks are well reproduced (see Fig. 7**a**). Especially, the structure factors predicted by all these techniques exhibit a good match with experimental data in the high-Q domain, which echoes the fact MD, RMC, and FEAR all offer a fairly realistic description of the short-range order structure of the glass. On the other hand, we observe the existence of some discrepancies in the low-Q region between the structure factor predicted by MD and experimental data (see

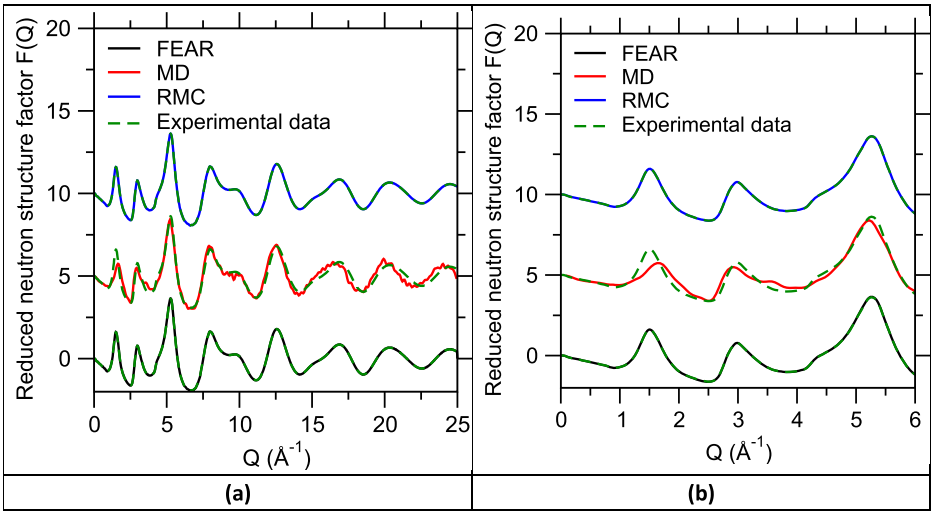

Fig. 7. (a) Reduced neutron structure factor of the glassy silica structures generated by force-enhanced atomic refinement (FEAR), molecular dynamics (MD, using a cooling rate of 1 K/ps), and reverse Monte Carlo (RMC) simulation. The data are compared with the same experimental neutron diffraction data [52]. Panel **(b)** shows a zoom of the low-*Q* domain of the same structure factors.

Fig. 7**b**). In particular, the intensity and degree of asymmetry of the first-sharp diffraction peak (FSDP) around 1.5 Å $^{-1}$ is not well predicted by MD. This suggests that MD offers a poor description of the medium-range order structure of the glass. In contrast, we find that both RMC and FEAR refinements offer a significantly improved description of the low-*Q* region of the structure factor. Importantly, the intensity, position, and the degree of asymmetry of the FSDP are well-reproduced by RMC and FEAR. This suggests that, although the level of structural refinement enabled by FEAR (and RMC) does alter the Si–O–Si angular distribution (see Fig. 6**c**), the refinement primarily affects the medium-range order structure of the simulated glass. Specifically, the fact that FEAR predicts a sharper FSDP than MD suggests that the glass refined using FEAR exhibits a more ordered medium-range structure than its MD-based counterpart—which is the main structural feature that may explain the increased stability (i.e., lower energy) of the FEAR-based glass.

In glassy silica, the medium-range order is primarily encoded in the ring size distribution, wherein silicate rings are defined as the shortest closed paths made of Si–O bonds within the atomic network [9,55]. To further explore how the enhanced thermodynamic stability enabled by FEAR refinement finds its origin in the medium-range order of the glass structure, we compute the ring size distribution of each model by using the RINGS package [55] while using the Guttman's definition for the rings' calculation (see Section 2.6).

Fig. 8**a** presents the ring size distribution computed by FEAR, RMC, and MD simulations. We note that the ring size distribution predicted by MD is in good agreement with previous works [19,26,52,66], being centered around 5-to-6-membered rings—wherein the ring size is expressed in terms of the number of Si atoms it comprises. However, we observe some differences between the ring size distributions predicted by MD, RMC, and FEAR. Notably, we observe that FEAR yields a sharper ring size distribution than that predicted by MD, which, once again, highlights the fact that the glass generated by FEAR exhibits a more ordered medium-range order structure than its MD counterpart. This result echoes previous findings obtained for a sodium silicate glass [41]. The sharpening of the ring size distribution observed herein is also in agreement with recent MD results, which showed that the ring size distribution tends to become sharper upon decreasing cooling rate, that is, as the glass becomes more stable [22].

Although no direct measurement of the ring size distribution is available to date to validate the computed ring size distributions for 3D silica glass [67], these results can be compared with the outcomes of the RingFSDP approach introduced by Shi et al. [18,68]. In brief, this method consists in deconvoluting the FSDP of the structure factor into the contribution of three types of rings: small (4-membered and smaller), intermediate (5-membered), and large (6-membered and larger)—which makes it possible to estimate the fraction of these three families of ring. Fig. 8**b** shows the computed fractions of small,

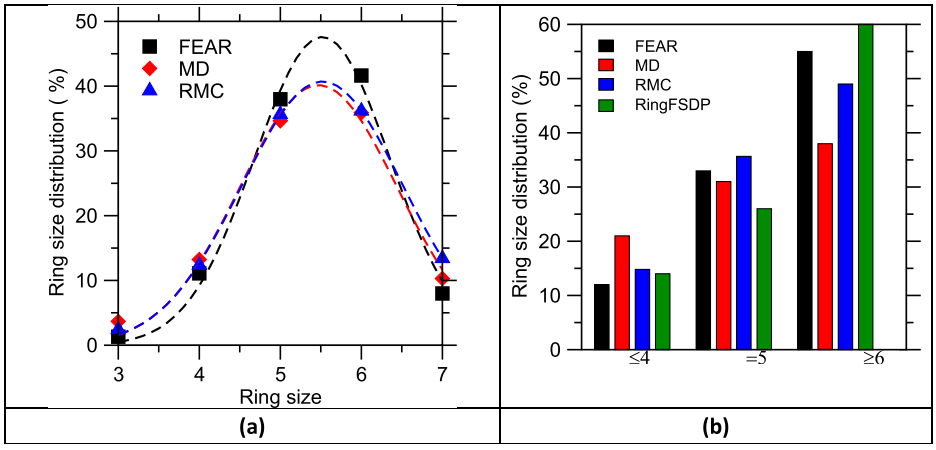

Fig. 8. (a) Ring size distribution of the glassy silica structures generated by force-enhanced atomic refinement (FEAR), molecular dynamics (MD, using a cooling rate of 1 K/ps), and reverse Monte Carlo (RMC) simulation. The dashed lines are to guide the eye. **(b)** Computed fractions of small (≤ 4-membered), intermediate (5-membered), and large (≥ 6-membered) rings in the glassy silica structures generated by FEAR, MD, and RMC. The data are compared with reference data inferred from diffraction data using the RingFSDP method [52].

intermediate, and large rings predicted by MD, RMC, and FEAR. When compared with MD results, we find that FEAR refinement results in (i) a decrease in the fraction of small rings and (ii) an increase in the fraction of large rings. Both of these behaviors are well supported by the outcomes of the RingFSDP analysis [52]. This confirms that FEAR yields a realistic description of the medium-range order structure of glassy silica.

The fact that FEAR predicts a lower fraction of small rings echoes the fact that such small rings, due to their topologically-over constrained nature, have been noted to be unstable due to the existence of small atomic-level internal stress [22]. Hence, small rings tend to disappear as the glass relaxes toward lower energy states [22]. This disappearance of small rings resulting from FEAR refinement (as compared to MD) is also in agreement with the increase in the average Si–O–Si angle observed in Fig. 6**b**. Indeed, it has been reported that small rings are associated with strained, smaller Si–O–Si angle, which is another signature of the fact that small rings are experiencing some internal stress. Overall, these results suggest that the stable nature of the glasses generated by FEAR largely arises from the fact that such glasses exhibit a more ordered medium-range order structure featuring fewer unstable small rings.

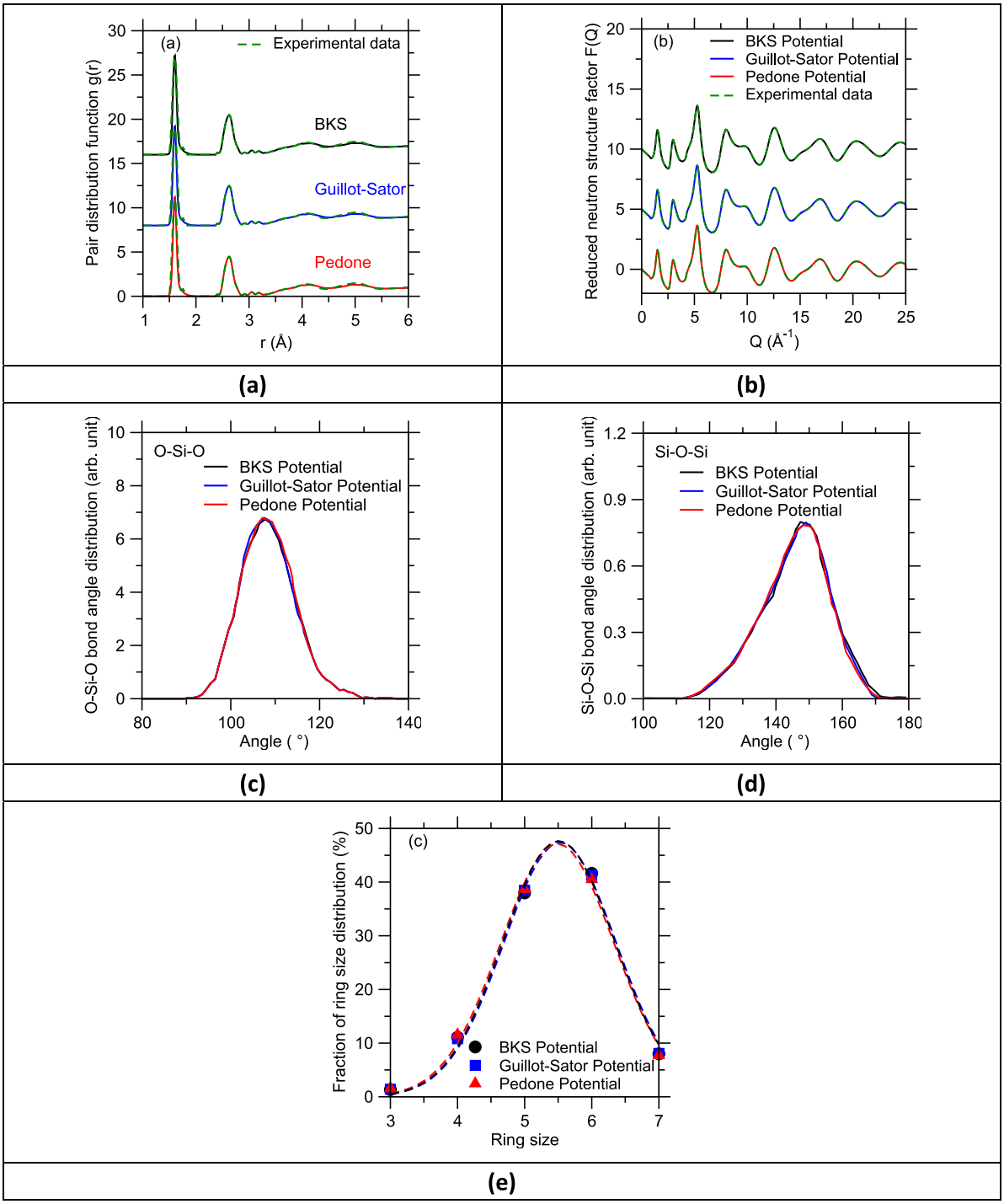

Fig. 9. Comparison of the **(a)** pair distribution function, **(b)** reduced neutron structure factor $F(Q)$, **(c)** O–Si–O, **(d)** Si–O–Si partial bond angle distributions, and **(e)** ring size distribution computed by FEAR while using different interatomic potentials. The structure factors are compared with the same experimental from neutron diffraction data [52].

4. Discussion

Finally, we discuss to which extent the outcome of FEAR refinement depends on the used interatomic forcefield. This is an important question since, for instance, the structure of glasses simulated by MD simulations strongly depends on the details of the interatomic potential that is used [69]. To this end, Fig. 9**a–e** shows the pair distribution function, reduced neutron structure factor, bond angle distributions, and ring size distribution predicted by FEAR while using three distinct interatomic potentials (see Methods section). Overall, we find that all these potentials yield virtually the same pair distribution function, neutron structure factor, bond angle distribution and, importantly, the same ring size distribution. This contrasts with the case of MD simulations, wherein the forcefield has a direct and significant impact on the simulated structure. Specifically, in MD simulations, the Si–O–Si partial bond angle and ring size distributions are often very sensitive to the choice of the interatomic forcefield. The fact that the outcome of the FEAR simulation does not notably depend on the choice of the interatomic potential can be understood from the fact that, in FEAR, the structure is mostly determined by the RMC steps, but only weakly impacted by the energy minimization. Rather, here, the energy minimizations solely ensure that the structure never deviates too much from an energetically stable state upon RMC refinement. Overall, in the FEAR approach, the role of the interatomic potential is only to discriminate stable from unstable structures generated by RMC, which effectively mitigates the ill-defined nature of RMC refinement. This suggests that FEAR simulations are not largely sensitive to the choice of the interatomic potential that is used and that, in contrast to MD simulations, even a poorly parameterized forcefield might yield realistic results when used within the FEAR approach.

5. Conclusions

All these results demonstrate that FEAR offers an improved description of the atomic structure of glassy silica as compared to traditional MD simulations based on the melt-quench method or RMC simulations. This is evident from the fact that FEAR yields a glass that simultaneously exhibits enhanced agreement with available experimental data and increased energetic stability. Overall, we find that the increased stability enabled by FEAR primarily arises from the fact that the generated glass exhibits a more ordered medium-range order structure and a lower fraction of unstable small silicate rings, which, in turn, tends to induce an opening of the Si–O–Si inter-tetrahedral angle. These results establish FEAR as a promising technique to "invert" available experimental into realistic, stable glass structures and to overcome the intrinsic limitations of traditional MD simulations. Importantly, unlike MD simulations, FEAR simulations are not very sensitive to the details of the interatomic potential that is used. This suggests that FEAR could be used to simulate a wide array of glass families, even in the absence of a robust interatomic forcefield. Overall, this approach could leapfrog one's ability to reveal the hidden atomic structure of complex disordered materials.

CRediT authorship contribution statement

Qi Zhou: Conceptualization, Methodology, Investigation, Writing – original draft, Writing – review & editing. **Ying Shi:** Writing – review & editing, Supervision. **Binghui Deng:** Writing – review & editing, Supervision. **Tao Du:** Methodology, Software, Validation. **Lijie Guo:** Writing – review & editing, Funding acquisition. **Morten M. Smedskjaer:** Writing – review & editing, Supervision. **Mathieu Bauchy:** Conceptualization, Writing – review & editing, Supervision, Project administration, Funding acquisition.

Declaration of Competing Interest

The authors declare that they have no known competing financial interests or personal relationships that could have appeared to influence the work reported in this paper.

Acknowledgments

Q.Z. acknowledges the Co-op program provided by Science and Technology Division of Corning Inc., which allowed her to conduct this study. The authors acknowledge financial support for this research provided by the National Science Foundation under Grant No. CMMI-1826420 and DMR-1928538, and the International Cooperation on Scientific and Technological Innovation Programs of BGRIMM under Grant No. 2017YFE0107000. M.M.S. acknowledges funding from the Independent Research Fund Denmark (Grant No. 7017-00019).

References

[1] J.C. Mauro, Decoding the glass genome, Curr. Opin. Solid State Mater. Sci. 22 (2018) 58–64, https://doi.org/10.1016/j.cossms.2017.09.001.
[2] J.C. Mauro, C.S. Philip, D.J. Vaughn, M.S. Pambianchi, Glass Science in the United States: current status and future directions, Int. J. Appl. Glass Sci. 5 (2014) 2–15, https://doi.org/10.1111/ijag.12058.
[3] J.C. Mauro, E.D. Zanotto, Two centuries of glass research: historical trends, current status, and grand challenges for the future, Int. J. Appl. Glass Sci. 5 (2014) 313–327, https://doi.org/10.1111/ijag.12087.
[4] L. Wondraczek, J.C. Mauro, J. Eckert, U. Kühn, J. Horbach, J. Deubener, T. Rouxel, Towards ultrastrong glasses, Adv. Mater. 23 (2011) 4578–4586, https://doi.org/10.1002/adma.201102795.
[5] in: C.Le Losq, M.R. Cicconi, G.N. Greaves, D.R. Neuville, Silicate glasses (Eds.), in: J.D. Musgraves, J. Hu, L. Calvez (Eds.), Springer Handbook of Glass, Springer International Publishing, Cham, 2019, pp. 441–503, https://doi.org/10.1007/978-3-319-93728-1_13.
[6] Y. Yu, B. Wang, M. Wang, G. Sant, M. Bauchy, Revisiting silica with ReaxFF: towards improved predictions of glass structure and properties via reactive molecular dynamics, J. Non Cryst. Solids. 443 (2016) 148–154, https://doi.org/10.1016/j.jnoncrysol.2016.03.026.
[7] R.K. Biswas, P. Khan, S. Mukherjee, A.K. Mukhopadhyay, J. Ghosh, K. Muraleedharan, Study of short range structure of amorphous silica from PDF using Ag radiation in laboratory XRD system, RAMAN and NEXAFS, J. Non Cryst. Solids. 488 (2018) 1–9, https://doi.org/10.1016/j.jnoncrysol.2018.02.037.
[8] S.S. Sørensen, C.A.N. Biscio, M. Bauchy, L. Fajstrup, M.M. Smedskjaer, Revealing hidden medium-range order in amorphous materials using topological data analysis, Sci. Adv. 6 (2020) eabc2320, https://doi.org/10.1126/sciadv.abc2320.
[9] J. Du, A.N. Cormack, The medium range structure of sodium silicate glasses: a molecular dynamics simulation, J. Non Cryst. Solids. 349 (2004) 66–79, https://doi.org/10.1016/j.jnoncrysol.2004.08.264.
[10] S.R. Elliott, Medium-range structural order in covalent amorphous solids, Nature 354 (1991) 445–452, https://doi.org/10.1038/354445a0.
[11] R. Shi, H. Tanaka, Distinct signature of local tetrahedral ordering in the scattering function of covalent liquids and glasses, Sci. Adv. 5 (2019) eaav3194, https://doi.org/10.1126/sciadv.aav3194.
[12] P.Y. Huang, S. Kurasch, J.S. Alden, A. Shekhawat, A.A. Alemi, P.L. McEuen, J. P. Sethna, U. Kaiser, D.A. Muller, Imaging atomic rearrangements in two-dimensional silica glass: watching silica's dance, Science 342 (2013) 224–227, https://doi.org/10.1126/science.1242248.
[13] Y. Yang, J. Zhou, F. Zhu, Y. Yuan, D.J. Chang, D.S. Kim, M. Pham, A. Rana, X. Tian, Y. Yao, S.J. Osher, A.K. Schmid, L. Hu, P. Ercius, J. Miao, Determining the three-dimensional atomic structure of an amorphous solid, Nature 592 (2021) 60–64, https://doi.org/10.1038/s41586-021-03354-0.
[14] A. Pandey, P. Biswas, D.A. Drabold, Inversion of diffraction data for amorphous materials, Sci. Rep. 6 (2016) 33731.
[15] J. Du, L.R. Corrales, First sharp diffraction peak in silicate glasses: structure and scattering length dependence, Phys. Rev. B. 72 (2005), 092201, https://doi.org/10.1103/PhysRevB.72.092201.
[16] J. Du, L.R. Corrales, Compositional dependence of the first sharp diffraction peaks in alkali silicate glasses: a molecular dynamics study, J. Non Cryst. Solids. 352 (2006) 3255–3269, https://doi.org/10.1016/j.jnoncrysol.2006.05.025.
[17] M. Micoulaut, M. Bauchy, Anomalies of the first sharp diffraction peak in network glasses: evidence for correlations with dynamic and rigidity properties, Phys. Status Solidi B 250 (2018) 976–982, https://doi.org/10.1002/pssb.201248512.
[18] Y. Shi, J. Neuefeind, D. Ma, K. Page, L.A. Lamberson, N.J. Smith, A. Tandia, A. P. Song, Ring size distribution in silicate glasses revealed by neutron scattering first sharp diffraction peak analysis, J. Non Cryst. Solids 516 (2019) 71–81, https://doi.org/10.1016/j.jnoncrysol.2019.03.037.
[19] M. Bauchy, Structural, vibrational, and thermal properties of densified silicates: insights from molecular dynamics, J. Chem. Phys. 137 (2012), 044510, https://doi.org/10.1063/1.4738501.

[20] C. Massobrio, J. Du, M. Bernasconi, P.S. Salmon, Molecular Dynamics Simulations of Disordered Materials, Springer International Publishing, Cham, 2015, https://doi.org/10.1007/978-3-319-15675-0.

[21] J.M.D. Lane, Cooling rate and stress relaxation in silica melts and glasses via microsecond molecular dynamics, Phys. Rev. E 92 (2015), 012320, https://doi.org/10.1103/PhysRevE.92.012320.

[22] W. Song, X. Li, B. Wang, N.M. Anoop Krishnan, S. Goyal, M.M. Smedskjaer, J. C. Mauro, C.G. Hoover, M. Bauchy, Atomic picture of structural relaxation in silicate glasses, Appl. Phys. Lett. 114 (2019), 233703, https://doi.org/10.1063/1.5095529.

[23] J. Du, Challenges in molecular dynamics simulations of multicomponent oxide glasses, in: C. Massobrio, J. Du, M. Bernasconi, P.S. Salmon (Eds.), Molecular Dynamics Simulations of Disordered Materials, Springer International Publishing, Cham, 2015, pp. 157–180, https://doi.org/10.1007/978-3-319-15675-0_7. Netw. Glas. Phase-Change Mem. Alloys.

[24] L. Huang, J. Kieffer, Challenges in modeling mixed ionic-covalent glass formers, in: C. Massobrio, J. Du, M. Bernasconi, P.S. Salmon (Eds.), Molecular Dynamics Simulations of Disordered Materials, Springer International Publishing, Cham, 2015, pp. 87–112, https://doi.org/10.1007/978-3-319-15675-0_4. Netw. Glas. Phase-Change Mem. Alloys.

[25] X. Li, W. Song, K. Yang, N.M.A. Krishnan, B. Wang, M.M. Smedskjaer, J.C. Mauro, G. Sant, M. Balonis, M. Bauchy, Cooling rate effects in sodium silicate glasses: bridging the gap between molecular dynamics simulations and experiments, J. Chem. Phys. 147 (2017), 074501, https://doi.org/10.1063/1.4998611.

[26] K. Vollmayr, W. Kob, K. Binder, Cooling-rate effects in amorphous silica: a computer-simulation study, Phys. Rev. B. 54 (1996) 15808–15827, https://doi.org/10.1103/PhysRevB.54.15808.

[27] S. Plimpton, Computational limits of classical molecular dynamics simulations, Comput. Mater. Sci. 4 (1995) 361–364, https://doi.org/10.1016/0927-0256(95)00037-1.

[28] P. Bhaskar, R. Kumar, Y. Maurya, R. Ravinder, A.R. Allu, S. Das, N.N. Gosvami, R. E. Youngman, M.S. Bødker, N. Mascaraque, M.M. Smedskjaer, M. Bauchy, N.M. A. Krishnan, Cooling rate effects on the structure of 45S5 bioglass: insights from experiments and simulations, J. Non Cryst. Solids 534 (2020), 119952, https://doi.org/10.1016/j.jnoncrysol.2020.119952.

[29] L. Deng, J. Du, Effects of system size and cooling rate on the structure and properties of sodium borosilicate glasses from molecular dynamics simulations, J. Chem. Phys. 148 (2018), 024504, https://doi.org/10.1063/1.5007083.

[30] A. Tilocca, Cooling rate and size effects on the medium-range structure of multicomponent oxide glasses simulated by molecular dynamics, J. Chem. Phys. 139 (2013), 114501, https://doi.org/10.1063/1.4821150.

[31] S. Ito, T. Taniguchi, Effect of cooling rate on structure and mechanical behavior of glass by MD simulation, J. Non Cryst. Solids. 349 (2004) 173–179, https://doi.org/10.1016/j.jnoncrysol.2004.08.180.

[32] J. Tan, S. Zhao, W. Wang, G. Davies, X. Mo, The effect of cooling rate on the structure of sodium silicate glass, Mater. Sci. Eng. B 106 (2004) 295–299, https://doi.org/10.1016/j.mseb.2003.09.045.

[33] R.L. McGreevy, L. Pusztai, Reverse Monte Carlo simulation: a new technique for the determination of disordered structures, Mol. Simul. 1 (1988) 359–367, https://doi.org/10.1080/08927028808080958.

[34] R.L. McGreevy, Reverse Monte Carlo modelling, J. Phys. Condens. Matter 13 (2001) R877–R913, https://doi.org/10.1088/0953-8984/13/46/201.

[35] P. Biswas, R. Atta-Fynn, D.A. Drabold, Reverse Monte Carlo modeling of amorphous silicon, Phys. Rev. B (2004) 69, https://doi.org/10.1103/PhysRevB.69.195207.

[36] C. Bousige, A. Boţan, F.J. Ulm, R.J.M. Pellenq, B. Coasne, Optimized molecular reconstruction procedure combining hybrid reverse Monte Carlo and molecular dynamics, J. Chem. Phys. 142 (2015), 114112, https://doi.org/10.1063/1.4914921.

[37] G. Opletal, T. Petersen, B. O'Malley, I. Snook, D.G. McCulloch, N.A. Marks, I. Yarovsky, Hybrid approach for generating realistic amorphous carbon structure using metropolis and reverse Monte Carlo, Mol. Simul. 28 (2002) 927–938, https://doi.org/10.1080/089270204000002584.

[38] D.A. Keen, R.L. McGreevy, Structural modelling of glasses using reverse Monte Carlo simulation, Nature 344 (1990) 423–425, https://doi.org/10.1038/344423a0.

[39] C.R. Müller, V. Kathriarachchi, M. Schuch, P. Maass, V.G. Petkov, Reverse Monte Carlo modeling of ion conducting network glasses: an evaluation based on molecular dynamics simulations, Phys. Chem. Chem. Phys. 12 (2010) 10444, https://doi.org/10.1039/c003472j.

[40] D.A. Drabold, Topics in the theory of amorphous materials, Eur. Phys. J. B 68 (2009) 1–21, https://doi.org/10.1140/epjb/e2009-00080-0.

[41] Q. Zhou, T. Du, L. Guo, M.M. Smedskjaer, M. Bauchy, New insights into the structure of sodium silicate glasses by force-enhanced atomic refinement, J. Non Cryst. Solids 536 (2020), 120006, https://doi.org/10.1016/j.jnoncrysol.2020.120006.

[42] A. Pandey, P. Biswas, D.A. Drabold, Force-enhanced atomic refinement: structural modeling with interatomic forces in a reverse Monte Carlo approach applied to amorphous Si and SiO_2, Phys. Rev. B (2015) 92, https://doi.org/10.1103/PhysRevB.92.155205.

[43] D.K. Limbu, R. Atta-Fynn, D.A. Drabold, S.R. Elliott, P. Biswas, Information-driven inverse approach to disordered solids: applications to amorphous silicon, Phys. Rev. Mater. 2 (2018), https://doi.org/10.1103/PhysRevMaterials.2.115602.

[44] Z. Liu, Y. Hu, X. Li, W. Song, S. Goyal, M. Micoulaut, M. Bauchy, Glass relaxation and hysteresis of the glass transition by molecular dynamics simulations, Phys. Rev. B 98 (2018), 104205, https://doi.org/10.1103/PhysRevB.98.104205.

[45] G.J. Kramer, N.P. Farragher, B.W.H. van Beest, R.A. van Santen, Interatomic force fields for silicas, aluminophosphates, and zeolites: derivation based on ab initio calculations, Phys. Rev. B 43 (1991) 5068–5080, https://doi.org/10.1103/PhysRevB.43.5068.

[46] F. Yuan, L. Huang, Brittle to ductile transition in densified silica glass, Sci. Rep. 4 (2015) 5035, https://doi.org/10.1038/srep05035.

[47] R.W. Hockney, J.W. Eastwood, Computer simulation using particles, in: 1966.

[48] B. Guillot, N. Sator, A computer simulation study of natural silicate melts. Part I: low pressure properties, Geochim. Cosmochim. Acta 71 (2007) 1249–1265, https://doi.org/10.1016/j.gca.2006.11.015.

[49] A. Pedone, G. Malavasi, M.C. Menziani, A.N. Cormack, U. Segre, A new self-consistent empirical interatomic potential model for oxides, silicates, and silica-based glasses, J. Phys. Chem. B 110 (2006) 11780–11795, https://doi.org/10.1021/jp0611018.

[50] S. Plimpton, Fast parallel algorithms for short–range molecular dynamics, (n.d.) 42.

[51] W.G. Hoover, Canonical dynamics: equilibrium phase-space distributions, Phys. Rev. A. 31 (1985) 1695–1697, https://doi.org/10.1103/PhysRevA.31.1695.

[52] Y. Shi, D. Ma, A.P. Song, B. Wheaton, M. Bauchy, S.R. Elliott, Structural evolution of fused silica below the glass-transition temperature revealed by *in-situ* neutron total scattering, J. Non Cryst. Solids. (2019), 119760, https://doi.org/10.1016/j.jnoncrysol.2019.119760.

[53] V.F. Sears, Neutron scattering lengths and cross sections, Neutron News 3 (1992) 26–37, https://doi.org/10.1080/10448639208218770.

[54] A.C. Wright, The comparison of molecular dynamics simulations with diffraction experiments, J. Non Cryst. Solids 159 (1993) 264–268, https://doi.org/10.1016/0022-3093(93)90232-M.

[55] S.Le Roux, P. Jund, Ring statistics analysis of topological networks: new approach and application to amorphous GeS_2 and SiO_2 systems, Comput. Mater. Sci. 49 (2010) 70–83, https://doi.org/10.1016/j.commatsci.2010.04.023.

[56] L. Guttman, Ring structure of the crystalline and amorphous forms of silicon dioxide, J. Non Cryst. Solids. 116 (1990) 145–147, https://doi.org/10.1016/0022-3093(90)90686-G.

[57] P.G. Debenedetti, F.H. Stillinger, Supercooled liquids and the glass transition, Nature 410 (2001) 259–267, https://doi.org/10.1038/35065704.

[58] W. Kob, H.C. Andersen, Testing mode-coupling theory for a supercooled binary Lennard-Jones mixture I: the van Hove correlation function, Phys. Rev. E 51 (1995) 4626–4641, https://doi.org/10.1103/PhysRevE.51.4626.

[59] A.C. Wright, Neutron scattering from vitreous silica. V. The structure of vitreous silica: what have we learned from 60 years of diffraction studies? J. Non Cryst. Solids 179 (1994) 84–115, https://doi.org/10.1016/0022-3093(94)90687-4.

[60] J. Neuefeind, K.D. Liss, Bond angle distribution in amorphous germania and silica, Ber. Bunsenges. Für Phys. Chem. 100 (1996) 1341–1349, https://doi.org/10.1002/bbpc.19961000812.

[61] W.J. Malfait, W.E. Halter, R. Verel, 29Si NMR spectroscopy of silica glass: T1 relaxation and constraints on the Si–O–Si bond angle distribution, Chem. Geol. 256 (2008) 269–277, https://doi.org/10.1016/j.chemgeo.2008.06.048.

[62] R.F. Pettifer, R. Dupree, I. Farnan, U. Sternberg, NMR determinations of Si O Si bond angle distributions in silica, J. Non Cryst. Solids. 106 (1988) 408–412, https://doi.org/10.1016/0022-3093(88)90299-2.

[63] H.F. Poulsen, J. Neuefeind, H.B. Neumann, J.R. Schneider, M.D. Zeidler, Amorphous silica studied by high energy X-ray diffraction, J. Non Cryst. Solids. 188 (1995) 63–74, https://doi.org/10.1016/0022-3093(95)00095-X.

[64] L.F. Gladden, T.A. Carpenter, S.R. Elliott, 29 Si MAS NMR studies of the spin-lattice relaxation time and bond-angle distribution in vitreous silica, Philos. Mag. B 53 (1986) L81–L87, https://doi.org/10.1080/01418638608244284.

[65] P.G. Coombs, J.F. De Natale, P.J. Hood, D.K. McElfresh, R.S. Wortman, J. F. Shackelford, The nature of the Si-O-Si bond angle distribution in vitreous silica, Philos. Mag. B. 51 (1985) L39–L42, https://doi.org/10.1080/13642818508240582.

[66] J.P. Rino, I. Ebbsjö, R.K. Kalia, A. Nakano, P. Vashishta, Structure of rings in vitreous SiO_2, Phys. Rev. B 47 (1993) 3053–3062, https://doi.org/10.1103/PhysRevB.47.3053.

[67] P.Y. Huang, S. Kurasch, A. Srivastava, V. Skakalova, J. Kotakoski, A. V. Krasheninnikov, R. Hovden, Q. Mao, J.C. Meyer, J. Smet, D.A. Muller, U. Kaiser, Direct imaging of a two-dimensional silica glass on graphene, Nano Lett. 12 (2012) 1081–1086, https://doi.org/10.1021/nl204423x.

[68] Y. Shi, Q. Zhou, B. Deng, M. Bauchy, Experimental method to quantify the ring size distribution in silicate glasses and simulation validation thereof, (n.d.).

[69] M. Bauchy, Structural, vibrational, and elastic properties of a calcium aluminosilicate glass from molecular dynamics simulations: the role of the potential, J. Chem. Phys. 141 (2014), 024507, https://doi.org/10.1063/1.4886421.